Organization of Poly(ethylene oxide) Monolayers at the Air–Water Interface

J. A. Henderson† and R. W. Richards*

Interdisciplinary Research Centre in Polymer Science and Technology, Department of Chemistry, University of Durham, South Road, Durham DH1 3LE, U.K.

J. Penfold

ISIS Division, Rutherford-Appleton Laboratory, Didcot, Oxon OX11 OQX, U.K.

R. K. Thomas and J. R. Lu

Physical Chemistry Laboratory, South Parks Road, Oxford OX1 3QZ, U.K.

Received November 30, 1992; Revised Manuscript Received May 12, 1993

ABSTRACT: Poly(ethylene oxide) has been spread at the air–water interface and the organization of the layer investigated using surface pressure isotherms and neutron reflectometry. Surface pressure data lead to the conclusion that the spread polymer is in a thermodynamically favorable environment on pure water which becomes worse as magnesium sulfate is added to the aqueous subphase. However, Θ conditions have not been realized over the range of magnesium sulfate molarities used (0.4–0.8 M). Neutron reflectometry data have been analyzed using both optical matrix and kinematic approximation methods. These suggest that, at low surface concentrations (≤0.4 mg m^{-2}), the polymer can be described as a single layer which is much diluted by water. At higher concentrations (up to 1.0 mg m^{-2}), the polymer penetrates the subphase and the segment distribution normal to the interface is describable by a Gaussian concentration profile. As the deposited surface concentration increases, the polymer penetrates deeper into the subphase and the topmost layer concentration remains approximately constant. The layer thickness of the spread monolayer is considerably thicker than the equilibrium surface excess layer obtained in a *solution* of poly(ethylene oxide). When magnesium sulfate is present in the subphase, the layer thickness is decreased and the polymer concentration of the topmost layer increases considerably.

Introduction

The organization and dynamics of polymers spread at the air–water interface are but poorly understood. In recent years some increase in the understanding of such monolayers has been obtained by the application of surface quasi-elastic light scattering[1,2] and neutron reflectometry[3] in conjunction with careful analysis of surface pressure isotherms.[4,5] Although such spread monolayers are often viewed as confining the polymer molecules to a two-dimensional state, this is perhaps only true over a limited range of concentrations. In the application of scaling laws to surface pressure isotherms, two dimensionality is assumed to be valid over the whole range of the isotherm. The validity of this assumption appears to have been confirmed by the equation of state analysis of surface pressure isotherms of poly(methyl methacrylate) at the air–water interface.[4,5] We have previously reported the results of neutron reflectometry and surface quasi-elastic light scattering experiments on poly(methyl methacrylate) spread on water.[3,6] We were able to show that a single coherent layer of polymer appears to be formed, the water and air contents of which depend on the polymer concentration.

Poly(ethylene oxide) (PEO) is a water-soluble polymer which can also be spread on the surface of water. In solution a surface excess is formed and Glass[7] has speculated that the monolayer and the surface excess are essentially identical. Shuler and Zisman[8] in an extended series of surface pressure and surface potential studies attempted to ascertain the configuration of the PEO unit with respect to the water surface. Kawaguchi[9] concluded from surface quasi-elastic light scattering results that, above a critical surface concentration, looping of the molecules into the aqueous subphase takes place; this critical concentration is estimated as 0.4 mg m^{-2}. From a study of the influence of temperature on surface pressure isotherms for PEO, Kuzmenka and Granick[10] noted that at low surface coverage's there was a loss of entropy due to confinement of the molecules to two dimensions. At higher surface coverages there was a gain in entropy as the monolayer "collapsed" to a three-dimensional structure. Additionally, they also suggested that water ordered at the surface with the PEO subunits.

We report here experiments using neutron reflectrometry which attempt to ascertain the organization of PEO at the air–water interface by evaluating the thickness of the surface layers and suggesting the arrangement of PEO subunits and water molecules with respect to each other in the surface.

Theory of Neutron Reflectrometry

Aspects of theory which are pertinent to the experimental results and data analysis are given here. Detailed descriptions have been provided by Born and Wolf,[11] Lekner,[12] and Sears.[13] Thomas[14] has given an overview of the application of neutron reflectometry to polymer-bearing surfaces.

The intensity of neutrons specularly reflected from a smooth interface between phases 1 and 2 is determined by the neutron refractive index, n, of the phase on which the beam is incident, and the refractive index is given by

$$n = 1-\lambda^2\rho_2/2\pi \quad (1)$$

with λ being the wavelength of the incident neutron beam

* Author to whom correspondence should be addressed.
† Current address: Chemdal Ltd., East Street, Birkenhead, Merseyside L41 1FG, U.K.

0024-9297/93/2226-4591$04.00/0

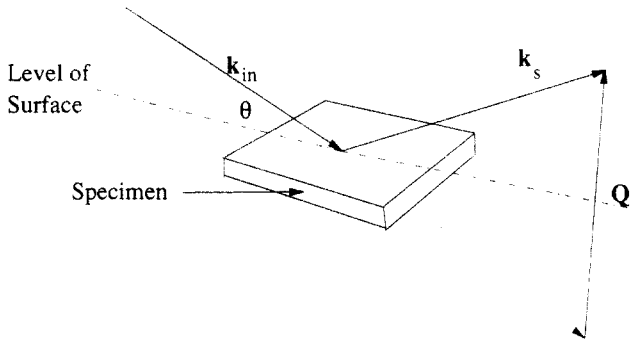

Figure 1. Definition of the scattering vector **Q** for a neutron beam of wave vector $\mathbf{k}_{in}$ ($\equiv 2\pi/\lambda$) incident on a surface at a glancing angle of θ.

and ρ_2 the scattering length density of the phase which has an atomic number density N. The scattering length density is the product of the coherent scattering length, b_i,[13] and the atomic number density, N_i, of each species present, i.e., $\rho_2 = \sum b_i N_i$. Total reflection takes place when the beam is incident at or below the critical angle, θ_c. Since $\cos(\theta_c) = n$ and θ_c is generally small, then $\theta_c/\lambda = (\rho_2/\pi)^{1/2}$. Rather than use angle as a variable, the more fundamental parameter is the scattering vector, **Q**, normal to the interface (Figure 1) and $|\mathbf{Q}|$ is defined as $(4\pi/\lambda)\sin\theta$; hence, $Q_c^2 = 16\pi\rho_2$. (This assumes that $\rho_1 = 0$, which is true where phase 1 is air; in the more general case, $Q_c^2 = 16\pi(\rho_2-\rho_1)$.) The Fresnel coefficient for the interface between the two phases, r_{12}, is

$$r_{12} = \frac{1-(1-Q_c^2/Q^2)^{1/2}}{1+(1-Q_c^2/Q^2)^{1/2}} \tag{2}$$

and the specular reflectivity at any value of Q for a smooth surface calculated from the Fresnel coefficients is

$$R_f(Q) = r_{12}^2 \tag{3}$$

where the surface has several layers of different n which are probed by the neutron beam; then the most efficient means of calculating the reflectivity is by defining an optical matrix for each layer using Abeles'[15] method. For the mth layer the optical matrix is defined by

$$M_m = \begin{vmatrix} \exp(i\beta_{m-1}) & r_m \exp(i\beta_{m-1}) \\ r_m \exp(i\beta_{m-1}) & \exp(-i\beta_{m-1}) \end{vmatrix} \tag{4}$$

where β_j is the optical path length in layer j (thickness d_j) defined as $(2\pi/\lambda)n_j d_j \sin\theta_j$ and r_m is the Fresnel coefficient for the interface between layers m and m-1. Multiplying all of these optical matrices produces a resultant matrix

$$\begin{bmatrix} M_{11} & M_{21} \\ M_{12} & M_{22} \end{bmatrix}$$

and the resultant specular reflectivity is given by

$$R(Q) = (M_{21}M_{21}^*)/(M_{11}M_{11}^*) \tag{5}$$

Use of such optical matrix methods in analyzing neutron reflectrometry data necessitates the adoption of a model for the surface layer or interface; the refractive index is then calculated from the distribution of matter at the interface and the calculated reflectivity compared with that observed.

Although the optical matrix methods described briefly above give the exact reflectivity, ambiguities arise since many models may fit the data and it is not easy to assess which model may be more appropriate. By contrast, the kinematic approximation is able to provide a more rapidly informative analysis of the data since subtle differences between surface structures are made more apparent. Although analysis using the kinematic approximation is still model dependent, it is less so than the optical matrix methods. The kinematic approximation is valid when $Q \gg Q_c$ and the reflectivity is weak.[16,17] In such circumstances,

Table I. Coherent Scattering Lengths ($\sum b_i$) and Scattering Length Densities (ρ)

substance	$\sum b_i/10^{-4}$ Å	$\rho/10^{-6}$ Å^{-2}
H_2O	−1.68	−0.56
D_2O	1.92	6.35
HPEO	0.41	0.57
DPEO	4.58	6.32

$$R(Q) = (16\pi^2/Q^2)|\rho(Q)|^2 \tag{6}$$

where $\rho(Q)$ is the one-dimensional Fourier transform of $\rho(z)$, the scattering length density distribution normal to the interface,

$$\rho(Q) = \int_{-\infty}^{\infty} \exp(-iQz)\rho(z)\,dz \tag{7}$$

and $\rho(z) = \sum_i b_i n_i(z)$ with $n_i(z)$ the number density distribution of species i at a distance z normal to the interface. Inserting eq 7 into eq 6 and writing $\rho(Q)$ in terms of $\sum b_i n_i(Q)$, then

$$R(Q) = (16^2/Q^2)\sum_i \sum_j b_i b_j h_{ij}(Q) \tag{8}$$

where $h_{jj}(Q)$ is known as the partial structure factor,[18] and when $i = j$, it describes the distribution of these species in the surface layer since

$$h_{ii}(Q) = |n_i(Q)|^2 \tag{9}$$

When $i \neq j$, then $h_{ij}(Q)$ will provide information on the distribution of species i and j relative to each other

$$h_{ij}(Q) = h_{ji}(Q) = \mathrm{Re}[n_i(Q)\, n_j^*(Q)] \tag{10}$$

Thus for poly(ethylene oxide) spread on the surface of water, the kinematic expression for the reflectivity is

$$R(Q) = (16\pi^2/Q^2)[b_{PEO}^2 h_{PEO}(Q) + b_{H_2O}^2 h_{H_2O}(Q) + 2b_{PEO}b_{H_2O}h_{pw}(Q)] \tag{11}$$

where $h_{pw}(Q)$ is the cross partial structure factor describing the correlation between polymer (p) and water (w). Provided enough systems with different values of b_i can be obtained, then all the $h_{ij}(Q)$ terms in eq 11 can be obtained. In certain cases the use of simplifying assumptions can be made which will enable almost as much information being obtained without the need for so many changes in b_i being necessary. Thomas et al.[17-19] have demonstrated the power of this approach in their work on partially deuterium-labeled surfactants. For poly(ethylene oxide) spread on water, the variation of scattering length density and coherent scattering length between the two constituents is sufficiently large (Table I) that the kinematic approximation can be successfully exploited. Underlying the use of selective deuterium labeling is the assumption that changing the level of deuteration has no influence on the structural organization. From small-angle neutron scattering on bulk polymers, deuteration certainly influences the thermodynamics especially in the region of a phase transition. However, Thomas et al.[28] have detected no difference in the surface tension or the area per molecule when the levels and loci of deuteration are altered. Additionally, the limiting areas per monomer obtained

Table II. Weight-Average Molecular Weights and Molecular Weight Distributions for Poly(ethylene oxides)

polymer	M_w[a]/10^3	M_w/M_n
HPEO	39.8	1.6
DPEO	35.6	2.0

[a] From light scattering in chloroform solutions.

for hydrogenous and deuterated PEO (vide infra) are equal within experimental error. Hence, there is a reasonable basis for presuming that, for the system studied here, deuteration has no influence on the surface layer structure.

Experimental Section

Synthesis of Poly(ethylene oxide). Ethylene oxide (Fluka) was transferred to a round-bottomed flask where it was stored over calcium hydride. The flask was attached to a high-vacuum line, the contents frozen by liquid nitrogen, and the flask evacuated. Repeated freezing and evacuation followed by thawing and prolonged stirring over calcium hydride were used for preliminary drying of the monomer. Immediately before use, the ethylene oxide was distilled into a second flask in which a sodium mirror had been formed. The monomer was gently swirled over the sodium mirror for an hour before being distilled onto a second sodium mirror where the process was repeated. Generally, exposure to 4 or 5 sodium mirrors was necessary before no tarnishing of the sodium was observed. The required amount of monomer was then distilled, under vacuum, into a round-bottomed flask fitted with a septum, followed by a sufficient volume of dry tetrahydrofuran to give a solution whose monomer concentration was between 5 and 10% w/w. The solution was warmed to a temperature of 195 K by immersing the flask in a mixture of dry ice and acetone. Diphenylmethylpotassium solution in tetrahydrofuran was used as the initiator, the requisite volume being injected through the septum on the flask. The flask and its contents were allowed to warm slowly to room temperature overnight and then held at 348 K for 4 days, after which time the solution was allowed to cool and the reaction terminated by injection of degassed glacial acetic acid through the septum. Pouring the resultant solution into a 10-fold excess of *n*-hexane produced the polymer as a precipitate which after filtration and drying was a fine powder.

An exactly similar procedure was used to prepare deuteropoly(ethylene oxide) using the deutero monomer (obtained from Merck, Sharp and Dohm) except for one additional step, which past experience had shown to be necessary. After treatment by sodium mirrors, the deutero monomer was distilled into a flask containing a few crystals of 9-fluorenone. A small volume (typically 15 μL) of 2.5 M *n*-butyllithium was then injected through a septum fitted to the flask. When a bright yellow color developed, the monomer was rapidly distilled off, leaving behind residual impurities and a trace of deuteropoly(ethylene oxide).

Weight-average molecular weights for the hydrogenous poly(ethylene oxide) (HPEO) and the deuterated poly(ethylene oxide) (DPEO) were obtained by low-angle laser light scattering using a Chromatix KMX6 photometer. Molecular weight distributions were obtained from aqueous phase size-exclusion chromatography. The results obtained are given in Table II.

Surface Pressure Isotherms. Isotherms of surface pressure (π) as a function of surface concentration (Γ_s) were obtained using an automatic recording surface film balance (trough area 900 cm^2) purchased from NIMA Technology, Coventry, U.K. This apparatus was placed on a vibration isolation table (Ealing Electro-Optics Ltd.), and temperature control was achieved by circulating water from an external thermostat through a labyrinth of channels in the poly(tetrafluoroethylene) base which forms the trough of the film balance. Typically, π/Γ_s isotherms were obtained by placing 20 μL of a solution of the polymer (DPEO or HPEO) in chloroform (1 mg mL^{-1}) on the surface of the aqueous subphase. The solvent was allowed to evaporate for 10 min and the surface pressure recorded as a function of surface concentration by closing the barriers at a constant speed (generally 30 cm^2 min^{-1}). In addition to investigating pure water as the subphase, π/Γ_s isotherms were also obtained using 0.4 M $MgSO_4$, 0.6 M $MgSO_4$, and 0.8 M $MgSO_4$ subphases. In common with pure water, these experiments were done at a temperature of 298 K, additional measurements were also made at 315 K using a subphase of 0.39 M $MgSO_4$, these later conditions defining Θ conditions for bulk solutions of poly(ethylene oxide). The water used in these experiments was first distilled and then passed through an Elgastat UHQ water purifier to produce water with a resistivity of 18 MΩ cm. Chloroform was of spectroscopic grade and the $MgSO_4$ an analytical grade reagent.

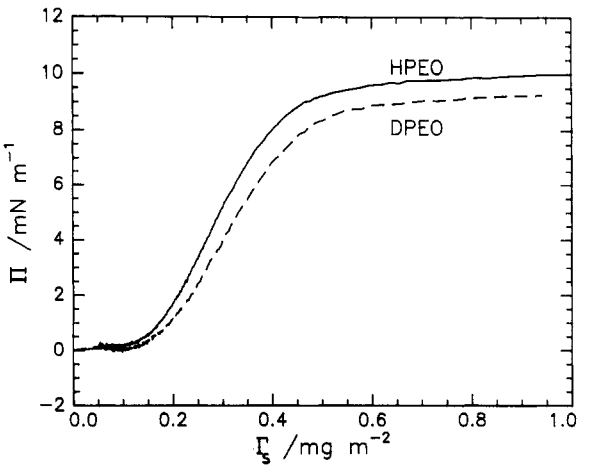

Figure 2. Surface pressure isotherms for HPEO and DPEO spread on water at 298 K.

Neutron Reflectrometry. All neutron reflectrometry profiles were obtained using the CRISP reflectometer, described elsewhere,[20] on the ISIS pulsed neutron source at the Rutherford-Appleton Laboratory, Oxfordshire, U.K. Because of the nature of the π/Γ_s isotherms (vide infra), it was anticipated that the polymer adopted an expanded configuration, with the possibility of any excursions into the subphase being to relatively large depths. Therefore, the reflectivity profiles were recorded over a wide range of Q, the scattering vector normal to the air–water interface. For the experiments reported here $0.01 \leq Q/Å^{-1} \leq 0.65$.

A rectangular poly(tetrafluoroethylene) trough was mounted in the neutron beam on a vibration isolation plinth, such that the compressing barriers were parallel to the incident beam direction. The trough was enclosed in a sealed aluminum box with quartz entrance and exit windows for the incident and reflected neutron beams. Holes in the top of the enclosure allowed access to the subphase surface for the deposition of the polymer film. All reflectrometry experiments were made at 294 K, and absolute reflectivities were obtained by scaling the data by a factor obtained from fitting the reflectivity profile obtained for D_2O using the known scattering length density of D_2O. For the experiments reported here, HPEO was spread on D_2O and DPEO was spread on a mixture of D_2O and H_2O with a scattering length density of 0. This latter subphase is termed null reflecting water. These two combinations were also used with the addition of $MgSO_4$ to the subphases. Only subphase salt molarities of 0.4 M $MgSO_4$ and 0.8 M $MgSO_4$ were investigated by neutron reflectrometry. The materials used were of quality identical to those used for the surface pressure isotherm studies except that D_2O obtained from Aldrich was used as received. The surface pressure was not monitored during reflectometry experiments.

For comparison purposes, neutron reflectometry measurements were also made on a solution of the same DPEO in null reflecting water. For this purpose a smaller trough without moving barriers was used and the concentration was 0.1% w/w.

Results

Surface Pressure. The π/Γ_s isotherms obtained for HPEO and DPEO are shown in Figure 2, both polymers have isotherms of the same type, i.e., liquid expanded. A higher equilibrium surface pressure of ca. 10 mN m^{-1} is displayed by HPEO, and this equilibrium value is attained

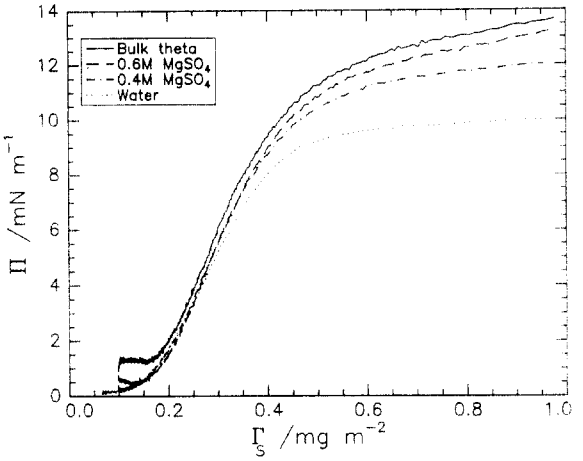

Figure 3. Surface pressure isotherms for HPEO spread on aqueous substrates with $MgSO_4$ molarities indicated. Bulk Θ indicates a subphase of 0.39 M $MgSO_4$ at a temperature of 315 K.

Table III. Area per Segment and *Values of y and υ* Obtained from Surface Pressure Isotherms

subphase	T/K	area per monomer/Å²	y	υ
H_2O	298	43	2.91	0.76
0.4 M $MgSO_4$	298	41	4.37	0.65
0.6 M $MgSO_4$	298	41	4.84	0.63
0.8 M $MgSO_4$	298	38	5.57	0.61
0.39 M $MgSO_4$	315	38	4.78	0.63

when $\Gamma_s \approx 0.6$ mg m^{-2}. By contrast DPEO has a slightly smaller equilibrium surface pressure of 9 mN m^{-1}. This small difference in surface pressure behavior is most probably due to the broader molecular weight distribution of the DPEO. Sauer and Yu[29] show surface pressure isotherms for monodisperse PEOs which differ depending on the molecular weight. By extrapolation to $\pi = 0$ of the linear portions of the isotherms of $0.2 \leq \Gamma_s \leq 0.4$ mg m^{-2}, the limiting area per monomer obtained is 43 Å^2 for both HPEO and DPEO. In view of this observation and the earlier remarks on the observed influence of deuteration on surfactant properties, we have not distinguished between HPEO and DPEO in the discussion of the neutron reflectometry results and we use the generic term PEO throughout. A numerical differentiation of these data shows the presence of an inflection point at $\Gamma_s \approx 0.3$ mg m^{-2} and at $\Gamma_s \approx 0.5$ mg m^{-2}, the latter point being where the equilibrium surface pressure is being approached. Although the initial concentration of PEO on the surface was ca. 0.07 mg m^{-2}, this is somewhat too high to be able to use the equation of state analyses of Singer[21] and Huggins[22] and be able to extract a number-average molecular weight and two-dimensional second virial coefficient from the data. However, from the slope of a double-logarithmic plot of the data the slope in the region $0.2 \leq \Gamma_s$/mg m$^{-2} \leq 0.4$ is obtained as 2.90 ± 0.01. This corresponds to the value of y in the equation $\pi \propto \Gamma_s^y$ obtained by application of scaling laws to surface pressure isotherms.[3-5,23]

Figure 3 shows the surface pressure isotherms for HPEO spread on aqueous subphases containing dissolved magnesium sulfate. Increasing the salt content of the subphase increases the equilibrium surface pressure, which is indicative of more polymer being in the immediate surface layer, i.e., a denser packing of segments. The area per monomer (obtained by extrapolation as described above) also decreases as the subphase is changed (Table III) from pure water to 0.8 M $MgSO_4$; however, the decrease is not large. The value of y obtained from double-logarithmic plots shows a marked dependence on the nature of the subphase (Table III) and reflects the change in the thermodynamics of the interaction between PEO and the subphase. Results for DPEO were identical to those obtained for HPEO except that the equilibrium surface pressure was marginally lower, as noted when pure water was used as the subphase.

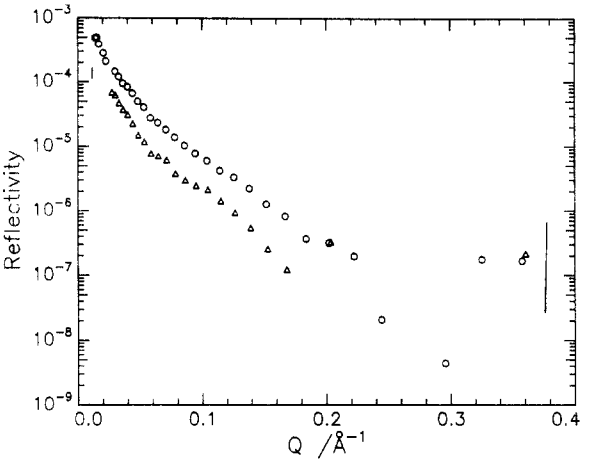

Figure 4. Reflectivity profile obtained after background subtraction for DPEO on null reflecting water: (○) $\Gamma_s = 0.8$ mg m^{-2}, (△) $\Gamma_s = 0.3$ mg m^{-2}. Vertical lines indicate error limits from counting statistics.

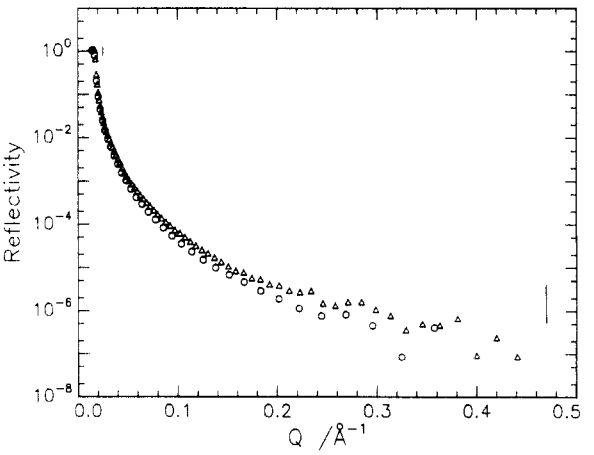

Figure 5. Reflectivity profiles obtained after background subtraction for HPEO spread on D_2O: (○) $\Gamma_s = 0.8$ mg m^{-2}, (△) $\Gamma_s = 0.2$ mg m^{-2}. Vertical lines indicate propagated errors from counting statistics.

Neutron Reflectometry. Reflectometry profiles for DPEO on a null reflecting water subphase are shown in Figure 4. The specular reflectivity decreases rapidly with increasing scattering vector, and this suggested that the surface layer was rather thick (>25 Å); however, the low values of the reflectivity are indicative of a low concentration of polymer in this layer or layers. This last point is reinforced by the reflectivity profiles for HPEO spread on D_2O (Figure 5). If the volume fraction of polymer in the layer is less than 0.5, which is what is expected here, the effect of the polymer would be to reduce the reflectivity as the surface concentration increases. A small decrease in the reflectivity is noted as the surface concentration of HPEO is increased; hence, the volume fraction of PEO in the monolayer is less than 0.5 over the whole range of Γ_s investigated.

In the analysis of these data to obtain quantitative descriptions of the PEO surface film, both the optical matrix method and the kinematic approximation have been used. In principle there are an infinite number of models which could be used to fit the reflectivity data;

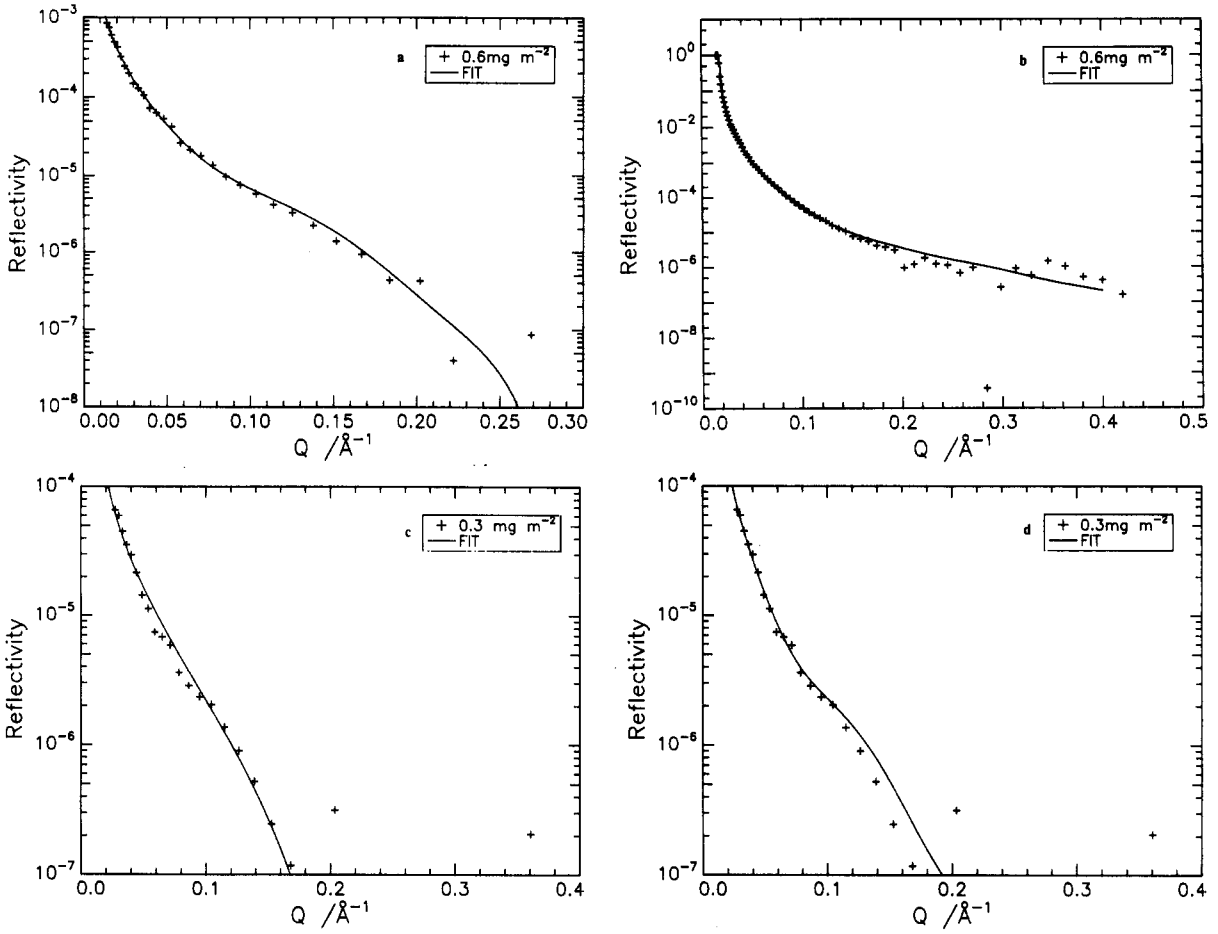

Figure 6. Representative fits of models to reflectivity profiles: (a) DPEO Γ_s = 0.6 mg m^{-2} on null reflecting water, two layers; (b) HPEO Γ_s = 0.6 mg m^{-2} on D_2O, two layers; (c) DPEO Γ_s = 0.3 mg m^{-2} on null reflecting water, two layers; (d) DPEO Γ_s = 0.3 mg m^{-2} on null reflecting water, single layer. Background subtracted from all plots.

however, earlier work on *solutions*[24] of PEO had suggested that the surface excess in such solutions had a two-layer structure. Consequently, this suggests that a model of the surface film of PEO as a single layer on the surface will not be successful. We have used two models to fit the data using the optical matrix method, these models are (i) two discrete layers and (ii) a Gaussian concentration profile at the surface. An exponential concentration profile was also attempted but gave poor fits and is not discussed further here.

In fitting the two-layer model the following strategy was adopted: the thickness of the layer in contact with the air (d_1) was fixed, and the scattering length density of this layer and the second lower layer, ρ_1, and ρ_2, respectively, were used as adjustable fitting parameters together with d_2, the thickness of the lower layer. The residual of the fit was noted and then the procedure repeated with a new value of d_1. By plotting the residuals as a function of d_1, a minimum residual could be identified associated with a particular value of d_1. Each of the other parameters (ρ_1, ρ_2, and d_2) were adjusted in a similar way to give an optimized set of values; however, this procedure was unsuccessful in obtaining an acceptable fit to the reflectivity data for the highest value of Γ_s investigated by reflectometry (0.8 mg m^{-2}). Examples of fits to the reflectometry data are shown in Figure 6. For each layer, the scattering length density, obtained from fitting to the reflectrometry data for DPEO on null reflecting water, is related to the volume fraction (ϕ) of polymer in the layer by the equation

$$\rho_i = \rho_{\mathrm{DPEO}}\phi^i_{\mathrm{DPEO}} \qquad (12)$$

where i = 1 or 2. In a similar fashion, the scattering length densities obtained from the reflectivity of the HPEO on D_2O are given by

$$\rho_i = \rho_{\mathrm{HPEO}}\phi^i_{\mathrm{HPEO}} + \rho_{\mathrm{D_2O}}\phi^i_{\mathrm{D_2O}} \qquad (13)$$

and since ρ_{HPEO}, $\rho_{\mathrm{D_2O}}$, and ϕ^i_{HPEO} are known, the latter quantity being equal to ϕ^i_{DPEO}, then the volume fraction of D_2O in each of the two layers can be calculated. Furthermore, both the scattering length density and the layer thickness can be used to calculate the area per monomer unit and thus the surface concentration, Γ_s^c

$$\text{area per momomer unit} = \sum b_i/\rho d \qquad (14)$$

$$\text{calculated surface concentration} = (m/N_A)\rho d/\sum b_i \qquad (15)$$

with $\sum b_i$ being the sum of the coherent scattering lengths of the atoms in the monomer unit, m the molecular weight of the monomer unit, and N_A Avogadro's number. For this two-layer model, the area per monomer unit was calculated by summing the product ρd over both layers. Thicknesses of the two layers, their volume fraction compositions, and the calculated surface concentrations are given in Table IV. The upper layer thickness is approximately constant at ca. 22 Å, and the volume fraction of polymer in this upper layer increases as Γ_s increases, becoming constant at $\Gamma_s \approx 0.6$ which approximates closely to the surface concentration where the asymptotic value of the surface pressure is rapidly approached. There appears to be no air contained in this layer, and the water volume fraction shows a slight decrease as Γ_s increases. The deeper second layer appears to be twice as thick, with

Table IV. Layer Thicknesses, Volume Fraction Compositions, and Calculated Surface Concentration from the Fit of a Two-Layer Model to Reflectometry Data

Γ_s/mg m^{-2}	layer 1			layer 2			Γ_s^c/mg m^{-2} [a]
	d_1/Å	ϕ^1_{PEO}	$\phi^1_{H_2O}$	d_2/Å	ϕ^2_{PEO}	$\phi^2_{H_2O}$	
0.8[b]							
0.7	24 ± 2	0.19	0.83	48 ± 8	0.02	0.99	0.58
0.6	23 ± 2	0.19	0.90	43 ± 8	0.02	0.99	0.58
0.5	24 ± 2	0.18	0.83	55 ± 8	0.01	0.97	0.56
0.4	22 ± 2	0.17	0.84	35 ± 10	0.03	0.96	0.51
0.3	24 ± 2	0.11	0.87	49 ± 10	0.01	0.99	0.36
0.2	17 ± 3	0.03	0.95	47 ± 10	0.04	0.99	0.28

[a] Calculated surface concentration from values of d and ρ obtained from fitting to reflectivity data. [b] No values reported because fits to data gave physically unrealistic values.

Table V. Characteristic Decay Length, Volume Fraction Composition, and Calculated Surface Concentration for a Gaussian Distribution of Poly(ethylene oxide)

Γ_s/mg m^{-2}	d_{char}/Å	ϕ_{PEO}	ϕ_{H_2O}	Γ_s^c/mg m^{-2}
0.8	18 ± 2	0.2	0.79	0.52
0.7[a]				
0.6	14 ± 2	0.28	0.86	0.54
0.5	16 ± 2	0.23	0.78	0.49
0.4	20 ± 2	0.18	0.83	0.51
0.3	19 ± 3	0.12	0.84	0.32
0.2	21 ± 5	0.09	0.96	0.26

[a] No values reported because fits to data gave physically unrealistic values.

a thickness of ca. 45 ± 10 Å, but the volume fraction of PEO in this second layer is very low at ca. 0.01–0.02. Although this two-layer model gives reasonable fits to the reflectometry data (Figure 6), it should be pointed out that, for low values of Γ_s (0.2–0.4 mg m^{-2}), the residuals of the fits to the data were of the same order as a fit of a single-layer model. At higher values of Γ_s (0.5–0.7 mg m^{-2}), the residuals from the fit of the two-layer model were always considerably smaller than those of the one-layer model. Furthermore, we note that the value of the surface concentration calculated from the reflectometry values consistently overestimates the surface concentration until Γ_s reaches 0.6, where the reflectometry parameters then underestimate Γ_s.

The two-layer model is somewhat physically unrealistic, and consequently we have also used a model where there is a Gaussian distribution of polymer segments into the aqueous subphase. For this model the form of the scattering length density profile is subdivided into n layers and the scattering length density of each layer is given by

$$\rho_i = \rho_1 \text{ factor} + \rho_{(n+1)}(1 - \text{factor}) \tag{16}$$

with ρ_1 being the scattering length density of the uppermost layer and $\rho_{(n+1)}$ being the scattering length density of the bulk subphase, and factor = $\exp(-4x^2/d_{char}^2)$ where $d_{char}/2$ is the full width of the half Gaussian, describing the polymer concentration profile, at 1/e of its height, and x is the distance into the subphase. This profile was divided into n strips of thickness d_{char}/n with n having a value of 20. (This value of n=20 was chosen as the smallest value of n above which the smoothness of the reflectivity profile was not improved by having a larger number of thinner layers.) The values obtained for d_{char} by fitting this profile to reflectivity data and the volume fraction composition of the layers are given in Table V. Residuals from the fitting of this function were of the same order of magnitude as those obtained with the discrete two-layer model. Moreover, the calculated surface concentrations are closer to the actual surface concentrations except for the highest value of Γ_s investigated.

The use of the optical matrix method provides the overall thickness and composition of the layer but does not give a direct insight into the distribution of the PEO segments or water at the surface. This can be obtained from the partial structure factor for each component using the kinematic approximation. In using the kinematic approximation, we are able to make some simplifying assumptions. First, for those cases where DPEO was spread on null reflecting water (b_{H_2O} = 0), then eq 11 simplifies to

$$R(Q) = (16\pi^2/Q^2) b_{PEO}{}^2 h_{PEO}(Q) \tag{17}$$

For HPEO spread on D_2O, the coherent scattering length for HPEO is sufficiently small that it can be approximated to 0 and thus

$$R(Q) = (16\pi^2/Q^2) b_{D_2O}{}^2 h_{D_2O}(Q) \tag{18}$$

At Q = 0, then from eq 9, $h_{PEO}(Q)$ should be the number density of PEO segments at an infinite depth from the surface and it should be zero as long as there is no dissolution of the polymer into the subphase. Rather than plot $h_{ij}(Q)$ as a function of Q, it is more informative to plot $Q^2 h_{ij}(Q)$ since this quantity is proportional to $Q^4 R(Q)$ which is a constant equal to the square of the difference in the scattering length density between air and subphase in the absence of any surface layer.[25] To calculate $h_{ij}(Q)$ from reflectometry data, the background from bulk scattering must first be subtracted. For our data here the background was calculated from the average specular reflectivity observed for the six highest Q values used. Crowley[26] has shown that the reflectivity that should be used in eq 11 (and hence eqs 18 and 19) is the value of $R(Q)$ in the equation

$$R(Q) - R_k(Q) = \left[\frac{1 + (1 - Q_c^2/Q^2)^{1/2}}{2}\right]^2 \left[\frac{R_{obs}(Q) - R_f(Q)}{1 - R_f(Q)}\right] \tag{19}$$

where $R_{obs}(Q)$ is the reflectivity observed experimentally, $R_k(Q)$ is the reflectivity calculated via the kinematic approximation for a smooth interface between the two bulk phases in the absence of any surface layer (eq 6), and $R_f(Q)$ is the Fresnel reflectivity for the same interface calculated by eq 3. For the bulk phases we have

$$R_k(Q) = (16\pi^2/Q^2)\Delta\rho^2 \tag{20}$$

where $\Delta\rho = \rho_1^\infty - \rho_2^\infty$, i.e., the difference in scattering length densities at infinite distances within phases 1 and 2. For null reflecting water, eq 19 is exact since the refractive index difference with air is zero. When D_2O is the bulk phase, the corrections using eq 20 may be appreciable. However, even this correction fails when Q_c is approached too closely and data correction must be restricted to reflectivities less than ca. 5×10^{-3}. For the HPEO spread on D_2O data reported here, the correction of eq 20 has been made for reflectivities up to ca. 2×10^{-3}; all higher values of $R(Q)$ have been disregarded for the purposes of the kinematic approximation.

For DPEO monolayers spread on null reflecting water with a Gaussian distribution of segments with a number density described by

$$n_{pi} = n_{p1} \exp(-4x^2/d_{char}{}^2)$$

Table VI. Values of Γ_s^c, Characteristic Decay Length, and Uniform Layer Thickness from Partial Structure Factor Analysis of DPEO Monolayers on Null Reflecting Water

Γ_s/mg m^{-2}	Γ_s^c/mg m^{-2} [a]	d_{char}/Å[a]	Γ_s^c/mg m^{-2} [b]	τ/Å[b]
0.8	0.45	22 ● 2	0.4	23 ± 2
0.7[c]				
0.6	0.45	19 ± 2	0.43	24 ± 2
0.5	0.39	16 ± 2	0.36	17 ± 2
0.4	0.41	23 ● 2	0.35	23 ● 2
0.3	0.27	26 ± 4	0.25	27 ± 4
0.2	0.24	50 ● 15	0.28	69 ● 15

[a] Values for Gaussian concentration profiles. [b] Values for a uniform layer. [c] No values reported because fits to data gave physically unrealistic values.

then the product $Q^2h_{pp}(Q)$ is given by

$$Q^2h_{pp}(Q) \equiv \frac{Q^4R(Q)}{16\pi^2 b_{PEO}^2} = n_{p1}^2 \frac{\pi Q^2 d_{char}^2}{4} \exp\left(\frac{-Q^2 d_{char}^2}{8}\right) \quad (21)$$

where n_{p1} is the number density of PEO segments at the immediate air–water interface and d_{char} is the characteristic decay length of the Gaussian distribution. It was found that, for $\Gamma_s \leq 0.4$ mg m^{-2}, this model was a poor fit to the data and for these lower Γ_s values a single layer model was found to be a better fit. In this case,[19]

$$Q^2h_{pp}(Q) = 4n_{p1}^2 \sin^2(Q\tau/2) \quad (22)$$

where τ is the layer thickness. Values of Γ (calculated from n_{p1}), d_{char}, and τ for both models are given in Table VI, and examples of fits to the data are shown in Figure 7. Earlier we noted that the kinematic approximation is valid when the reflectivity is low. Figure 7 apparently shows that a good fit to the data can be obtained over the whole range of Q. However, because the reflectivity is multiplied by Q^2 in the plots of Figure 7, then as Q approaches small values near zero the deviations become greatly attenuated and hence agreement between model and data is observed.

Partial structure factor analysis can also be applied to determine the distribution of water at the surface where the distribution can be represented by

$$n_{si} = n_{so} \tanh(z/\xi) \quad (23)$$

when a Gaussian distribution of PEO segments is used and ξ characterizes the width of the distribution of water molecules at the surface and n_{so} is the number density of water at an infinite distance into the subphase. The expression used to fit the data is then

$$Q^2h_{ww}(Q) = \frac{Q^4R(Q)}{16\pi^2 b_{D_2O}^2} = n_{so}^2(\xi\pi Q/2)^2 \operatorname{cosech}^2\left(\frac{\xi\pi Q}{2}\right) \quad (24)$$

In using eq 24, n_{so}^2 was fixed at the bulk number density of water (1.1×10^{-3} Å^{-6}). For $0.2 \leq \Gamma_s$/mg m$^{-2} \leq 0.4$, a single uniform layer model was found to be a better fit to the data, and for this situation we have

$$Q^2h_{ww}(Q) = \frac{Q^4R(Q)}{16\pi^2 b_{D_2O}^2} = n_{so}^2 + 4n_{s1}(n_{s1} - n_{so}) \sin^2(Q\sigma/2) \quad (25)$$

where n_{s1} is the number density of water in the surface layer of thickness σ. For $0.2 \leq \Gamma_s$/mg m$^{-2} \leq 0.4$, the value of n_{s1} was found to be slightly less than n_{so} and the layer thickness is of the same order as that of the PEO layer and suggests that the water is spread uniformly throughout the PEO layer. A typical fit to the data is given in Figure 8, and Table VII gives the values of the parameters obtained (n_{s1}, ξ, and σ).

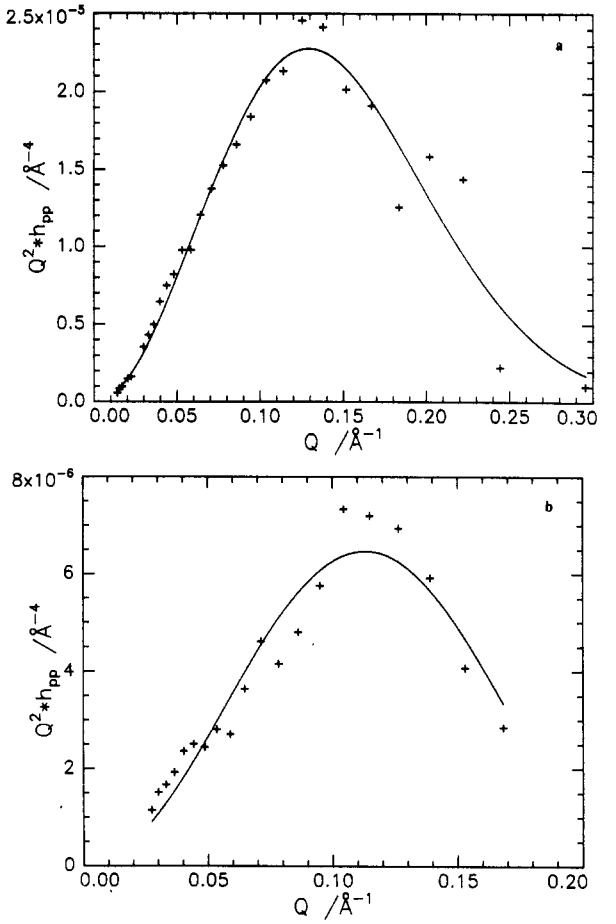

Figure 7. Partial structure factor plots (Q^2h_{ii}) for DPEO on null reflecting water. h_{pp} is the partial structure factor for DPEO (see eq 9): (a) $\Gamma_s = 0.8$ mg m^{-2}, Gaussian distribution of segments; (b) $\Gamma_s = 0.3$ mg m^{-2}, single uniform layer. Solid line is the fit to the data.

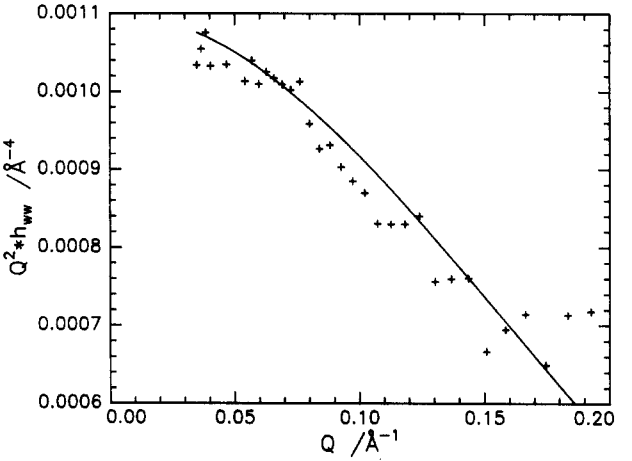

Figure 8. Partial structure factor for the distribution of D_2O at the surface for HPEO monolayer $\Gamma_s = 0.6$ mg m^{-2}. h_{ww} is the partial structure factor for D_2O.

The kinematic approximation has been used exclusively to analyze the reflectivity data obtained for PEO spread on aqueous $MgSO_4$ subphases. However, satisfactory fits could not be obtained for $\Gamma_s = 0.2$ mg m^{-2} for both the 0.4 M $MgSO_4$ and 0.8 M $MgSO_4$ subphases for either the Gaussian profile or the single-layer model. In common with the pure water subphase, for $\Gamma_s \leq 0.4$ mg m^{-2} the single-layer model gave the better fit; for higher values of

Table VII. Values of Characteristic Decay Length, Uniform Layer Thickness, and Number Density of Water in the Surface Layer from Partial Structure Factor Analysis of HPEO Monolayers on D_2O

Γ_s/mg m^{-2}	ξ/Å	σ/Å	n_{s1}/Å^{-3}
0.8	4 ± 1	14 ± 2	0.026
0.7[a]			
0.6	5 ± 1	16 ± 2	0.029
0.5	5 ± 1	16 ± 2	0.026
0.4	4 ± 1	17 ± 2	0.027
0.3	4 ± 1	18 ± 2	0.027
0.2	4 ± 1	19 ± 2.0	0.032

[a] No values reported because fits to data gave physically unrealistic values.

Table VIII. DPEO on Aqueous $MgSO_4$ Solutions with Values of Γ_s^c, Characteristic Decay Length, and Uniform Layer Thickness from Partial Structure Factor Analysis

Γ_s/mg m^{-2}	Γ_s^c/mg m^{-2} [a]	d_{char}/Å[a]	Γ_s^c/mg m^{-2} [b]	τ/Å[b]
	(a) Subphase 0.4 M $MgSO_4$			
0.8	0.40	14 ± 2	0.37	16 ± 2
0.7	0.48	17 ± 2	0.47	19 ± 2
0.6	0.39	9 ± 1	0.39	11 ± 2
0.5	0.39	10 ± 1	0.41	11 ± 2
0.4	0.29	10 ± 1	0.37	13 ± 2
0.3[c]				
0.2[c]				
	(b) Subphase 0.8 M $MgSO_4$			
0.8	0.45	10 ± 1	0.48	11 ± 1
0.7	0.45	10 ± 1	0.45	11 ± 1
0.6	0.45	11 ± 1	0.44	13 ± 1
0.5	0.49	13 ± 2	0.49	17 ± 2
0.4	0.44	17 ± 3	0.45	15 ± 2
0.3	0.35	12 ± 3	0.32	14 ± 3
0.2[c]				

[a] Values for a Gaussian concentration profile. [b] Values for a uniform layer. [c] No values reported because fits to data gave physically unrealistic values.

Γ_s the Gaussian distribution was better. The values of Γ, d_{char}, and τ obtained for each model are given in Table VIII. The values of ξ, σ, and n_{s1} for the distribution of water when aqueous $MgSO_4$ was the subphase were unchanged from those obtained in the absence of $MgSO_4$ and previously given in Table VII.

An informative comparison can be made between the spread monolayer with Γ_s = 0.8 mg m^{-2} and the surface excess of DPEO which develops in null reflecting water. Assuming that a Gaussian concentration profile describes the surface excess, then for such a distribution of DPEO segments

$$\Gamma_s^c = d_{char} n_{p1} \pi^{1/2}/2 \text{ molecules Å}^{-2} \quad (26)$$

Replacing in eq 21 and rearranging, then

$$\ln(h_{pp}(Q)) = 2 \ln \Gamma_s^c - Q^2 d_{char}/8 \quad (27)$$

Figure 9 shows the reflectivity data for DPEO as a monolayer and as a solution with null reflecting water as the aqueous phase. The lines are least-squares fits to the data over the range $0.04 \le Q/\text{Å}^{-1} \le 0.2$, and both extrapolate to the same value of Γ_s^c which is 0.45 ± 0.05 mg m^{-2}. However, the slopes of the two lines are considerably different. For the spread monolayer the slope gives a d_{char} value of 22 Å in agreement with the value in Table VI. The d_{char} value for the surface excess layer in the solution is much smaller at 17 Å, a value which is well outside the experimental error of ±2 Å. Figure 9 also illustrates the departure of the kinematic approximation for reflectivities obtained at $Q < 0.04$ Å^{-1} which was remarked on earlier.

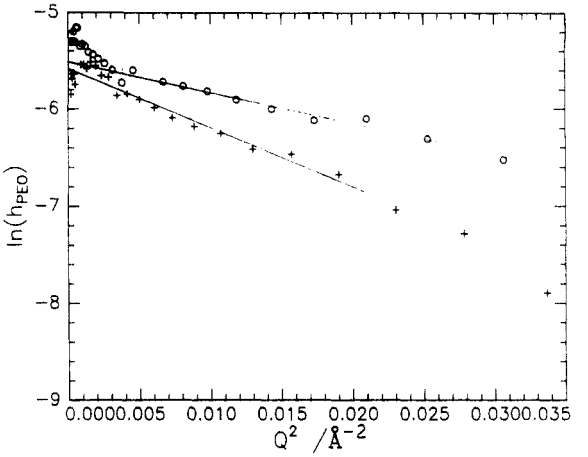

Figure 9. Partial structure factor data for DPEO plotted according to eq 27: (O) 0.1% solution of DPEO on null reflecting water; (+) 0.8 mg m^{-2} spread layer of DPEO on null reflecting water.

Discussion

From the value of the exponent y obtained (Table III) relating the dependence of π on Γ_s we can draw some conclusions regarding the nature of the thermodynamic state of the PEO monolayer. Scaling laws[27] relate y to the exponent υ in the relation between the radius of gyration and molecular weight via the equation $y = 2\upsilon/(2\upsilon-1)$. The values of υ obtained are also given in Table III; for pure water we obtain υ = 0.76 which is in excellent agreement with the accepted value of 0.75[4,5] for a polymer in thermodynamically good solvent conditions. (In an earlier paper[3] we have commented on the relative intensity of y with regard to the value of υ.) A decrease in υ is observed as the molarity of the $MgSO_4$ increases but never attains the value of 0.57 which is the generally accepted value for a two-dimensional polymer in the Θ state. It is also noteworthy that the bulk Θ solvent (0.39 M $MgSO_4$ at 315 K) is by no means a Θ medium for the PEO monolayer and indicates a surface depletion of magnesium sulfate in the bulk subphase.

For PEO spread on pure water the overall description obtained from a consideration of the various models used to fit the data is that a surface concentrations ≤ 0.4 mg m^{-2} the PEO exists as a single layer on the water surface and contains water but at a considerably lower concentration than bulk. The volume fraction of polymer in this single layer increases from ca. 0.09 to 0.2 over this range of Γ_s. The data which confirms this view are the observation that Γ_s^c calculated from NR data is in very good agreement with the amount spread, Γ_s. For higher values of Γ_s some of the PEO penetrates the subphase where it is highly diluted by the water. Although a discrete two-layer model can be fitted to the data, a more realistic model is that of a Gaussian distribution of PEO segments since this retains the characteristics of the two-layer model without an abrupt change in concentration. This Gaussian model is supported by the results obtained from the use of the kinematic approximation. Of more interest in the results of the latter analysis is the direct insight it provides for the distribution of PEO segments and water molecules at the surface. Figure 10 shows the number density distribution for both PEO segments and water at low and high values of Γ_s. Furthermore, the kinematic approximation provides a value for the number density of polymer segments in the topmost layer (n_{p1}), and we note that this value becomes approximately constant for $\Gamma_s \ge 0.5$ mg m^{-2} which is also where the surface pressure rapidly approaches an asymptotic value at this value of Γ_s and

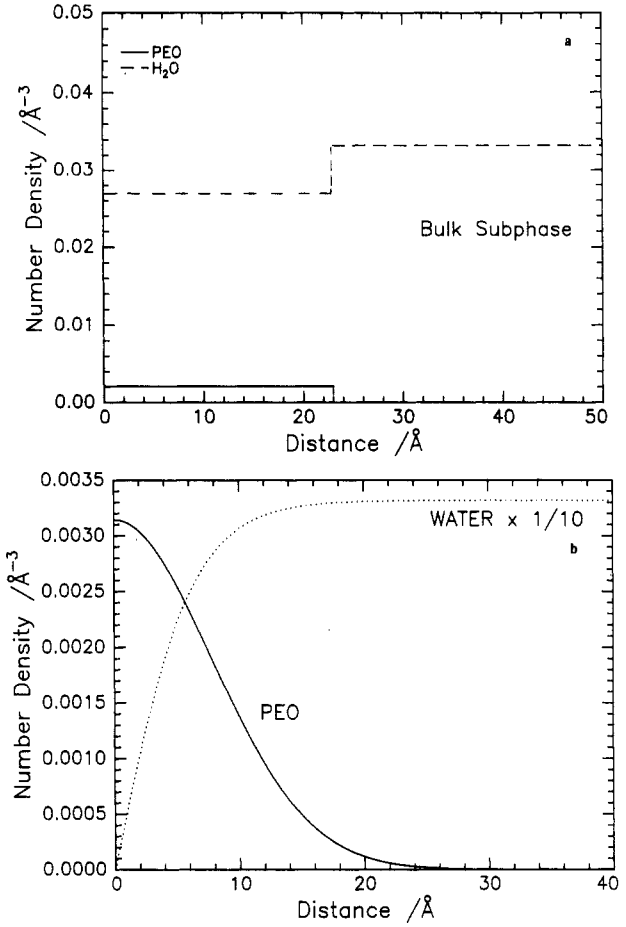

Figure 10. Number density distribution of PEO and water obtained from: (a) single uniform layer partial structure factor analysis for Γ_s = 0.3 mg m^{-2}; (b) Gaussian distribution partial structure factor analysis for Γ_s = 0.8 mg m^{-2}.

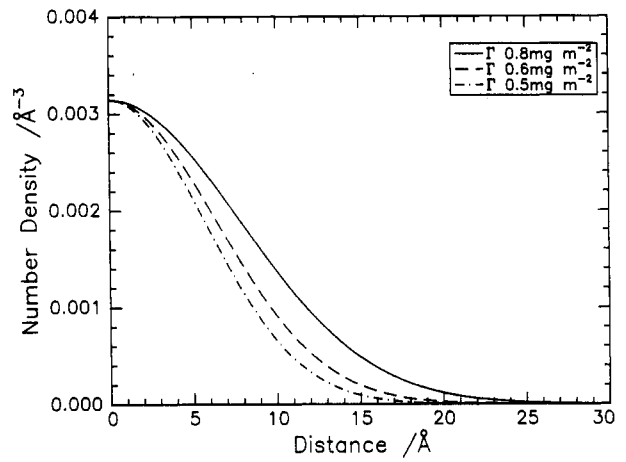

Figure 11. Number density distribution of PEO for Γ_s = 0.5, 0.6, and 0.8 mg m^{-2}. Parameters obtained from Gaussian profile and partial structure factor analysis.

the Gaussian model becomes a better description of the PEO monolayer. Hence, we conclude that, for $\Gamma_s \geq 0.5$ mg m^{-2}, the aqueous subphase can no longer accommodate more PEO segments on the surface and the molecules loop into the subphase. This may be due to the polymer adopting a highly extended configuration on the aqueous surface for low values of Γ_s due to the extremely favorable thermodynamic interaction with water. As Γ_s is increased above 0.5 mg m^{-2}, there is a small increase in the extension of PEO segments into the subphase (Figure 11), but the dimensions of the water layer remain essentially unaltered (Table VII).

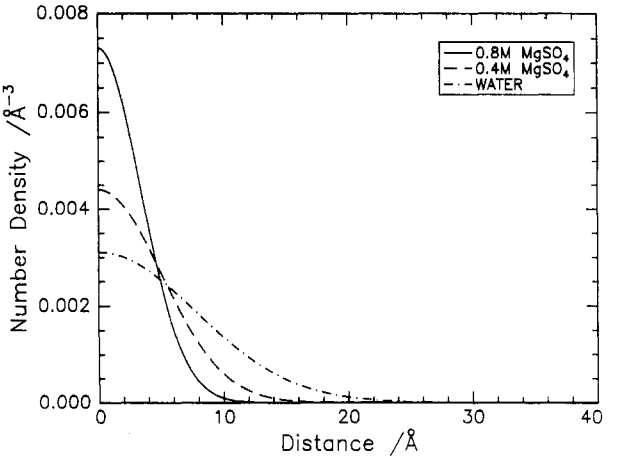

Figure 12. Influence of the molarity of $MgSO_4$ in subphase on the distribution of PEO segments.

When the subphase contains $MgSO_4$, the general effect is to decrease the thickness of the PEO layer and increase the concentration of PEO segments in the layer; i.e., there is a denser packing of PEO segments. For the lower values of Γ_s, the single-layer thickness is roughly half of that obtained in the absence of $MgSO_4$. At higher values of Γ_s, when 0.4 M $MgSO_4$ is the subphase, there is still an observable increase in the characteristic length due to extension of the PEO segments deeper into the subphase, although this extension is not as great as when pure water is the subphase. When the subphase is 0.8 M $MgSO_4$, the Gaussian distribution has a constant characteristic length of ca. 10 Å. The introduction of $MgSO_4$ into the subphase also greatly increases the number density of PEO segments at the air–subphase interface, almost doubling it when 0.8 M $MgSO_4$ is used as the subphase, but the reduction in layer thickness maintains the value of Γ_s[c]. The net effect of this increase in concentration and decrease in the characteristic length as the $MgSO_4$ content increases is shown in the number density profiles of Figure 12 for Γ_s = 0.8 mg m^{-2}.

When the surface concentration of PEO is larger than 0.4 mg m^{-2}, the organization of the polymer at the interface is qualitatively similar to that observed for the surface excess in *solutions* of PEO.[24] However, the dimensions of the layer for the spread films are much reduced compared to those in the surface excess layer. For this latter case a two-layer model was used, with d_1 and d_2 being 45 and 75 Å, respectively, for a 0.1% solution of PEO; the volume fraction of polymer in each of these layers was 0.09 and ca. 0.02, respectively. A comparison with the data given in Table IV obtained by application of the two-layer model to the current data, suggests that for spread films the layers are half as thick but approximately twice as concentrated. Consequently, the question arises as to whether the spread monolayers were in true equilibrium with the subphase. Typically, a reflectometry experiment took 1.5–2 h to collect data of sufficiently good signal to noise ratio. Additionally, in one experiment for which Γ_s = 0.6 mg m^{-2}, repeated measurements of the reflectivity were made over a 14-h period; no difference in the profiles was observed. Finally, we make some remarks concerning the results of Sauer and Yu,[29] who examined both spread layers of PEO and the surface excess formed in solutions. Using surface quasi-elastic light scattering, the frequency and damping of the capillary waves was found to be identical for both cases. However, this should not be interpreted as evidence for the two situations having the same structure normal to the surface. First, the momentum transfer is in surface quasi-elastic light scattering directed along the

liquid surface. Second, the value of the wave vector used is such that the capillary wavelength probed was ca. 180 μm. Furthermore, it is the surface tension which has the greatest influence on the properties of the capillary waves, and this is determined by the concentration of the polymer at the air–water interface. As we have shown, both spread monolayer and surface excess can have the same surface coverage but very different near surface depth profiles. Surface quasi-elastic light scattering can give no information on the organization normal to the interface.

Conclusions

Neutron reflectometry has been applied to monolayers of poly(ethylene oxide) spread on water and on aqueous magnesium sulfate subphases. At low surface concentrations ($\leq$0.4 mg m^{-2}), the polymer exists as one layer but is appreciably diluted by the subphase. At higher surface concentrations polymer segments extend into the subphase probably as loops and tails. This extension increases as the surface concentration increases. Application of the kinematic approximation and using a Gaussian model for the higher surface concentrations show that above surface concentrations of 0.5 mg m^{-2} the number density of PEO segments in the topmost layer is constant. This coincides with the region where the surface pressure attains an almost constant value even though the apparent surface concentration (Γ_s) is increasing. The presence of magnesium sulfate in the subphase severely reduces the thickness of the diffuse polymer layer and markedly increases the concentration of polymer in the topmost layer. However, the nature of the polymer layer is essentially unaltered.

Acknowledgment. We thank the Science and Engineering Research Council for providing finances to purchase the surface film balance and the provision of neutron beam facilities at the Rutherford-Appleton Laboratory. J.A.H. also thanks them for provision of a maintenance grant.

References and Notes

(1) Kawaguchi, M.; Sauer, B. B.; Yu, H. *Macromolecules* **1989**, *22*, 1735.
(2) Langevin, D., Ed. *Light Scattering by Liquid Surfaces and Complementary Techniques*; Dekker: New York, 1992.
(3) Henderson, J. A.; Richards, R. W.; Penfold, J.; Shackleton, C.; Thomas, R. K. *Polymer* **1991**, *32*, 3284.
(4) Vilanove, R.; Poupinet, D.; Rondelez, F. *Macromolecules* **1988**, *21*, 2880.
(5) Poupinet, D.; Vilanove, R.; Rondelez, F. *Macromolecules* **1989**, *22*, 2491.
(6) Henderson, J. A.; Richards, R. W.; Penfold, J.; Thomas, R. K. *Macromolecules* **1993**, *26*, 65.
(7) Glass, J. E. *J. Phys. Chem.* **1968**, *72*, 4459.
(8) Shuler, R. L.; Zisman, W. A. *J. Phys. Chem.* **1970**, *74*, 1523.
(9) Kawaguchi, M.; Komatsu, S.; Matsuzumi, M.; Takahashi, A. *J. Colloid Interface Sci.* **1984**, *102*, 356.
(10) Kuzmenka, D. J.; Granick, S. *Macromolecules* **1988**, *21*, 779.
(11) Born, M.; Wolf, E. *Principles of Optics*, 6th ed.; Pergamon: Oxford, U.K., 1980.
(12) Lekner, J. *Theory of Reflectivity*; Nijhoff: Dordrecht, The Netherlands, 1987.
(13) Sears, V. F. *Neutron Optics*; Oxford University Press: New York, 1989.
(14) Thomas, R. K. In *Scattering Methods in Polymer Science*; Richards, R. W., Eds.; to be published.
(15) Heavens, O. *Optical Properties of Thin Films*; Butterworth: Kent, U.K., 1955.
(16) Als-Nielsen, J. *Z. Phys.* **1985**, *64*, 411.
(17) Crowley, T. L.; Lee, E. M.; Simister, E. A.; Thomas, R. K. *Physica* **1991**, *B173*, 143.
(18) Lu, J. R.; Simister, E. A.; Lee, E. M.; Thomas, R. K.; Rennie, A. R.; Penfold, J. *Langmuir*, in press.
(19) Simister, E. A.; Lee, E. M.; Thomas, R. K.; Penfold, J. *J. Phys. Chem.*, in press.
(20) Penfold, J.; Thomas, R. K. *J. Phys. Condens. Matter* **1990**, *2*, 1369.
(21) Singer, S. J. *J. Chem. Phys.* **1948**, *16*, 872.
(22) Huggins, M. L. *Kolloid Z.* **1973**, *251*, 449.
(23) Kawaguchi, M.; Yoshida, A.; Takahashi, A. *Macromolecules* **1983**, *16*, 956.
(24) Rennie, A. R.; Crawford, R. J.; Lee, E. M.; Thomas, R. K.; Crowley, T. L.; Roberts, S.; Qureshi, M. S.; Richards, R. W. *Macromolecules* **1989**, *22*, 3466.
(25) Russell, T. P. *Mater. Sci. Rep.* **1990**, *5*, 171.
(26) Crowley, T. L. *Phys. A*, in press.
(27) Carmesin, I.; Noolandi, J. *Macromolecules* **1989**, *22*, 1689.
(28) Lu, J. R.; Lee, E. M.; Thomas, R. K.; Penfold, J.; Flitch, S. L. *Langmuir*, in press. Lu, J. R.; Simister, E. A.; Thomas, R. K.; Penfold, J. *J. Phys. Chem.*, in press.
(29) Sauer, B. A.; Yu, H. *Macromolecules* **1989**, *22*, 786.